Digital Computer Laboratory
Massachusetts Institute of Technology
Cambridge, Massachusetts

SUBJECT: SWITCH-CORE ANALYSIS I

To: N. H. Taylor

From: A. Katz and E. A. Guditz

Date: November 4, 1952

Abstract: Data derived from an experimental study of ferritic switch-cores is interpreted in terms of linear coupled-circuit theory. Despite the over-simplification resulting from assumptions of linear, time-invariant behavior and of negligible eddy-current and capacitive effects, it is found that such a model enables one to explain reasonably well the empirical results. Evident from the analyses, both experimental and theoretical, is the fact that simplicity of construction and effectiveness of transformer action place mutually contradictory constraints on the design of a magnetic-matrix switch. Whereas the former requires "few" turns per switch-core winding (one, if possible), the latter requires "many" turns so that the winding impedances will be large compared to that of the load.

1.0 Introduction

A considerable effort has been devoted, both at the Laboratory and elsewhere, to experimental studies of the responses of ferromagnetic core materials to various signal inputs. Interest in such materials stems from the fact that they possess those properties, non-linearity and hysteresis, which are essential to memory and switching applications. However, it is these same properties which render difficult any quantitative description of the behavior of circuit elements depending on these properties. Hence, experimental studies are a necessary preliminary to an understanding of such elements.

In this note we present and interpret experimental data derived from a grossly macroscopic, or "black-box" investigation of the behavior of certain ferritic cores operated as elements in a magnetic-core memory system. It should be noted that the results presented herein are based on a relatively small number of cores, and, hence, any conclusions derived should be accepted with circumspection.

2.0 Experimental Results

2.01 General Remarks

Before describing the experiments performed, we remark that the ultimate objective of this research is a semi-rigorous procedure for the design of a magnetic-matrix switch for use as a selection device for a magnetic-core memory system. Figure 1 is a diagram of one form of such a matrix switch. Since the principles of operation of this switch have been adequately described elsewhere(1), we need merely remark that only one of the 2^n cores in the switch is not biased to saturation, and hence capable of producing an output when excited by the driver. A useful by-product of this research would be some sort of equivalent-circuit representation for the magnetic core elements used in the switch.

The environment in which the matrix switches operate is shown in Figure 2, which is a diagram of a selection system for a single digit plane of a magnetic-core memory array. Corresponding to the particular states of the n X-address (or Y-address) flip-flops, a certain set of drivers will so actuate the switch that only one, S_i (or S_j), of its 2^n cores is capable of transmitting energy to its load. In this way each switch selects one line of each of the two sets of co-ordinate lines, say X_i and Y_j, along which to apply a magnetomotive force of amplitude equal to half that required to switch a memory core. Only the memory core, M_{ij}, lying at the intersection of X_i and Y_j, will experience sufficient mmf to be switched-- provided that no inhibiting pulse is simultaneously applied by the Z-plane driver.

By abstracting to essentials we arrive at Figure 3 from which the scope of the design problem is evident. In this figure the following quantities are defined:

R_{g1} = Impedance of X and Y vacuum-tube (v.t.) drivers

R_{g2} = Impedance of Z-plane v.t. driver

L_1 = Network linking the X or Y v.t. drivers with switch cores S_i or S_j respectively. This includes the impedances reflected into the primary windings of S_i and S_j by other cores in their respective matrices.

L_2 = Network linking switch core S_i (or S_j) to the memory core M_{ij}. This includes the impedance of the unselected memory cores on the co-ordinate line X_i (of Y_j).

L_3 = Network linking the Z-plane v.t. driver with memory core M_{ij}. This includes the impedance of the remaining memory cores in the digit plane.

L_4 = Network linking memory core M_{ij} with the sensing unit. This includes any impedances reflected into the sensing winding as well as various noise sources (e.g., "delta" noise).

---

1. Olsen, K. H., "A Magnetic-Matrix Switch and Its Incorporation Into a Coincident Current Memory", Digital Computer Laboratory Report R-211.

2.01 General Remarks (Cont.)

Even if the switch and memory cores were characterized by linear transfer functions, the design of the system shown would hardly be a trivial problem. When the cores are characterized by the flux-mmf relation shown in Figure 4 (as indeed they must be for these applications), then it is evident that the design of such saturable-core transformers must be preceded by much experimental study.

2.02 Description of Experiments

Although the research described here is still in progress, it is felt that a publication of partial results at this time would serve as a basis for drawing tentative conclusions and as a stimulus to further thought. This research might be divided roughly into the following sets of experiments:

(1) a study of switch cores wound with relatively large numbers of turns,

(2) a study of switch cores wound with relatively small numbers of turns, and

(3) a study of the static hysteresis curves for ferritic core types MF-1118 (F259) and MF-1131 (F262).

The first two sets were conducted under essentially the same conditions. In each case an MF-1131 (F262) core, wound with N_1 primary turns and N_2 secondary turns, was used as a link between the Z-plane v.t. driver and the Z-plane winding which threaded all of the MF-1118 (F259) cores in memory plane No. 2 of Memory Test Set-up No. 2. A simplified diagram of the set-up used is shown in Figure 5. A "rectangular" pulse of current of amplitude I_1, with duration of 1.5 microseconds and rise-time of 0.15 to 0.30 microseconds is applied to the primary winding of the switch core. A pulse of current of peak amplitude I_2 from the secondary then drives, through the Z-plane winding, the entire digit plane of memory cores from state A (at $-\phi_r$ in the flux-mmf plane in Figure 4) to state B. The X and Y drivers remain de-energized throughout these experiments. It has been experimentally determined that the plane of 256 cores, when operated in this mode, may be approximated reasonably well by an equivalent load of a 1 ohm resistor in series with a 2-microhenry inductor. Although this set-up does not represent a realistic application of a saturable-core transformer, it does provide valuable information relating to its use for driving large numbers of memory cores.

The distinction between these two sets of experiments shall arbitrarily be defined as follows: if N_1 or N_2 is greater than 10 turns, then the cores have windings with "large" numbers of turns; otherwise, "small" numbers of turns.

2.02 Description of Experiments (Cont.)

Such a distinction is necessary because simplicity of construction of a matrix switch requires "few" turns per winding, while effective transformer action requires "many" turns per winding.

The first set of experiments involved the study of an MF-1131 ferritic transformer with its primary winding tapped at 10-turn intervals over the range ($10 \leq N_1 \leq 100$), and its secondary tapped at 1-turn intervals over the range ($1 \leq N_2 \leq 5$) and at 5-turn intervals over the range ($5 \leq N_2 \leq 50$). The amplitude of the primary current pulse (I_1) was held constant at 400 milliamperes while N_1 and N_2 were varied, and the peak amplitude of the secondary current pulse (I_2) was measured. These data are plotted in various forms in Graphs I through IV. The interpretation of these data is given in Section 3.0.

It is evident that when the three variables -- N_1, N_2, and I_1 -- are fixed, then the fourth variable, I_2, is determined. In view of the fact that co-incident current operation of a memory array using MF-1118 (F259) cores requires about 1.5 amperes per selected coordinate line, it is also evident that not every combination of the first three variables provides the required current drive, I_2, for the array. It was therefore decided (on the basis of the first experiments) to select certain favorable combinations of N_1 and N_2, and then vary I_1 while measuring I_2. The particular combinations chosen were:

(a) $N_1 : N_2 = 20 : 5$
(b) $N_1 : N_2 = 25 : 5$
(c) $N_1 : N_2 = 30 : 5$

and I_1 was varied over the range of 0.2 to 2 amperes. The results of these tests are shown in Graphs V and VI.

Although attention thus far has been centered primarily on the peak amplitude of the current pulses (or mmf pulses), it is obvious that the shapes and durations of these pulses are of equal importance. In order to observe the effect of variations in driving magnetomotive force on the secondary current pulse, photographs were taken of the outputs of the three cores listed above for the same range of I_1 as was used in the peak amplitude measurements. These results are also discussed in Section 3.0.

After conducting these experiments with saturable-core transformers having "many-turn" windings, we then investigated similar phenomena for the "few-turn" case. Seven MF-1131 ferritic cores were wound with different numbers of primary turns: ($N_1 = 4, 5, \ldots, 10$). For each of these cores, the number of secondary turns was varied in 1-turn steps over the range ($1 \leq N_2 \leq 10$), the amplitude of the primary current pulse was varied over $0.5 \leq I_1 \leq 2$ amperes, and the peak amplitude of the secondary

2.02 Description of Experiments (Cont.)

current pulse was then measured. Some of these results are presented in various forms in Graphs VII through XII. In the course of these experiments, some cursory estimates were made of changes in shape and duration of the output pulse of the switch-core with changes in N_2 and I_1.

The third set of experiments consisted merely of the tracing (by B. Frackiewicz) of the static hysteresis curves for the two core types mentioned.

3.0 Interpretation of Experimental Results

3.01 Linear Analysis of the Coupled-Circuit Problem

In attempting to analyze physical systems one frequently postulates an idealized model, the behavior of which can be described quantitatively. The validity of the model may then be tested by using the equations which govern the idealized system to predict the behavior of the real system. If the correlation between experimental and predicted behavior is reasonably good, then one is justified in continuing the use of the model in further studies -- provided, of course, that the simplifying assumptions underlying the model are never violated.

In our case, the physical system to be analyzed consists of a toroidal core of ferritic material on which three windings are wrapped. Two of these correspond to the conventional transformer windings, while the third is used to reset the core to its "normal" remanent state at $-\phi_r$ (see Figure 4). The similarity between the switch-core and the conventional transformer suggests that the same sort of analysis might apply to both. The major obstacles to this approach are (a) the distorting effects of eddy currents on the hysteresis curve, and (b) the non-linear relation between flux and mmf as the core material moves along the path ACDE from $-\phi_r$ to $+\phi_m$. Fortunately, each of these obstacles may be bypassed without too much difficulty.

The first we may dispose of by noting that the volume resistivities of the ferrites are extremely high compared to those of the metallic ribbons. This so restricts the flow of eddy currents that their effects, to a first approximation, may be neglected in ferritic cores. If we further assume that the magnetizing component of the primary current is small compared to the load component, then the instantaneous operating point in the flux-mmf plane may be determined by entering Figure 4 along

$$(NI)_{net} = N_1 I_1 - N_2 I_2. \qquad (3.1)$$

In doing so, one must bear in mind the magnetic history of the core.

3.01 Linear Analysis of the Coupled-Circuit Problem (Cont.)

Replacing the non-linear flux-mmf relation by one which is linear may be justified on the following basis. Preliminary investigation of switching time as a function of the amplitude of the net driving mmf has indicated that, if enough mmf has been applied to drive a ferritic core beyond the second "knee" of the hysteresis loop, there are only small decreases in switching time and small increases in peak secondary current with increasing mmf. This behavior was observed over a range of net mmfs of $2 \leq H_{net} \leq 14$ oersteds in three MF-1131 (F262) cores (for which the coercive force is about one oersted). This anomalous behavior with respect to switching time was observed under the conditions of an essentially constant load (Z-plane winding plus 0.5 ohms) and of constant rise-time (about 0.8 μsec) of the primary current pulse. If these facts are corroborated by further experiments, then there appears to be little reason for driving the core far into saturation since this will cost heavily in large vacuum-tube drivers, yet will buy little. If, on the basis of these considerations, the switch core is operated so as to minimize driver requirements (and at small attendant loss in efficiency of utilization), then we may replace the actual core by the ideal one shown in Figure 4. For our purposes we require that the slopes in the saturated regions be small (not necessarily zero as shown) compared to those in the unsaturated regions.

To recapitulate, our basic assumptions are:

(a) Eddy currents negligible,

(b) Linear flux-mmf relation, and

(c) Magnetizing current small.

To these we add, for simplicity of analysis only,

(d) Capacitive effects negligible.

(e) Winding resistances negligible.

It will now be shown that a fairly good dorrelation exists between the experimental results and those derived from a linear analysis based on these assumptions.

Referring to the iron-core coupled circuit of Figure 6, we can write the following voltage equations:

$$\left.\begin{aligned} e(t) &= R_s i_1 + L_1 \frac{di_1}{dt} - M \frac{di_2}{dt} \\ 0 &= - M \frac{di_1}{dt} + L_2 \frac{di_2}{dt} + R_L i_2 \end{aligned}\right\} \qquad (3.2)$$

Laplace-transforming these equations, we obtain (if initial conditions are zero):

$$\left.\begin{aligned} E(s) &= (R_s + sL_1)\ I_1(s) - sMI_2(s) \\ 0 &\neq - sM\ I_1(s) + (R_L + sL_2)\ I_2(s) \end{aligned}\right\} \qquad (3.3)$$

3.01 Linear Analysis of the Coupled-Circuit Problem (Cont.)

From the second of equations 3.3, we see that the relation between loop currents is

$$\frac{I_2(s)}{I_1(s)} = \frac{sM}{sL_2 + R_L} \qquad (3.4)$$

If leakage flux is small, then the self-inductance of a winding on a toroid may be written as:

$$L = \frac{2\mu_d A}{r} N^2 = K_1 N^2 \qquad (3.5)$$

where $\mu_d = \dfrac{dB}{dH}$ = differential permeability

r = mean radius of toroid

A = cross-sectional area of toroid

N = number of turns in winding.

Similarly, the mutual inductance between windings 1 and 2 of a transformer is

$$M_{12} = \frac{2\mu_d A^*}{r^*} N_1 N_2 = kK_1 N_1 N_2 \qquad (3.6)$$

where k = coefficient of coupling

Substituting these expressions into equation 3.4, we obtain

$$\frac{I_2(s)}{I_1(s)} = \frac{skK_1N_1N_2}{sK_1N_2^2 + R_L} \qquad (3.7a)$$

For $R_L \ll sL_2$

$$\frac{I_2(s)}{I_1(s)} \approx \frac{skK_1N_1N_2}{sK_1N_2^2} = \frac{kN_1}{N_2} \qquad \boxed{(3.7b)}$$

and for $R_L \gg sL_2$

$$\frac{I_2(s)}{I_1(s)} \approx \frac{skK_1N_1N_2}{R_L} = kK_2N_1N_2 \qquad \boxed{(3.7c)}$$

Note that equation 3.7b may also be derived by summing mmfs around the closed magnetic loop of the toroid. If exciting current is small and the core is operated in the linear unsaturated region of the hysteresis curve, then equation 3.1 becomes

$$(NI)_{net} = N_1I_1 - N_2I_2 \approx 0$$

3.01 Linear Analysis of the Coupled-Circuit Problem (Cont.)

When the core is driven into saturation the net mmf will be non-zero and positive.

In order to apply the approximate equations 3.7b and 3.7c to the analysis of the experimental curves, one must know the magnitudes of the impedances of the load and of the secondary winding of the switch core. As previously indicated the load appears to be one ohm in series with two microhenries. To this we now add the 1/2 ohm current-measuring resistor. For the frequency corresponding to a rise-time of 0.3 microseconds, the impedance of the load is

$$Z_L = \sqrt{(X_L)^2 + (R_L)^2}$$
$$= \sqrt{(10.45)^2 + (1.5)^2} \approx 10.5 \text{ ohms}$$

It will later be shown that, to a reasonable approximation, the self-inductance of the secondary is

$$L_2 = K_1 N_2^2 = 2.52 N_2^2 \text{ microhenries}$$

For the same frequency the load and secondary impedances will be equal when

$$N_2^2 = \frac{Z_L}{\omega K_1} = \frac{10.5}{13.1}$$

$$\text{or} \quad N_2 \approx 1 \text{ turn.}$$

In order to define regions of N_2 in which equations 3.7b and 3.7c are separately valid, we shall arbitrarily set the dividing lines as

$$Z_2 \ll Z_L \text{, when } N_2 \leq 1 \text{ turn}$$
$$Z_2 \gg Z_L \text{, when } N_2 \geq 4 \text{ turns.}$$

3.02 Interpretation of Data

With the aid of these approximate equations, we now attempt to predict what the experimental results depicted in Graph I* should be. There the peak secondary current (I_2) is plotted as a function of secondary turns (N_2) with primary current (I_1) constant and various values of primary turns (N_1). For N_2 small, equation 3.7c predicts (under these conditions) that

$$I_2 = (kK_2 N_1 I_1) N_2$$
$$= K_a N_2 \quad ;$$

* All graphs appear in sequence following Figure 8.

3.02 Interpretation of Data (Cont.)

while for N_2 large, equation 3.7b predicts that

$$I_2 = \frac{kN_1 I_1}{N_2} = \frac{K_b}{N_2}$$

The composite curve for Graph I should, as does Figure 7, show

(a) for small N_2, a linear relationship between I_2 and N_2,

(b) for large N_2, a hyperbolic relationship,

(c) for intermediate N_2, a compromise relationship as the two curves of a. and b. fair together.

Examination of Graph I shows that the experimental curves do indeed bear a marked resemblance to the composite curve for Figure 7. Since the leakage inductance and shunt capacitance increases with the number of turns in the winding, one should expect deviations of the actual from the theoretical results to increase with increasing N_1 and/or N_2. Although this fact is evident in Graph I, it is displayed even more conspicuously in Graphs II and III.

In the first is shown a plot of peak secondary current I_2 versus N_1 with I_1 constant and various values of N_2. From equation 3.7b

$$I_2 = \frac{kI_1}{N_2} N_1$$
$$= K_c N_1 \qquad \text{(for a given } N_2\text{)}$$

is the theoretical relation between I_2 and N_1. Since the families of curves in Graph II involve $N_2 > 4$ turns, this relation would hold were it not for the increase in leakage with increasing primary turns.

In Graph III a different aspect of the same data is shown. There is a plot of I_2 versus N_2 with I_1 constant and various values of the turns ratio -- $a = N_1 : N_2$.

For $Z_L \gg sL_2$ equation 3.7c gives

$$I_2 = kK_2 I_1 N_1 N_2 = (kK_2 I_1 \frac{N_1}{N_2}) \; N_2^2$$
$$= K_d N_2^2 \qquad \text{for a given } \frac{N_1}{N_2},$$

3.02 Interpretation of Data (Cont.)

and for $Z_L << sL_2$ equation 3.7b gives

$$I_2 = \frac{kN_1}{N_2} I_1$$

$$= K_e \qquad \text{for a given } \frac{N_1}{N_2} .$$

Although insufficient data was collected to check the parabolic relation for small N_2, the second relation between I_2 and N_2 may be observed. However, only over a limited region is the secondary current independent of secondary turns; only for small values of the turns ratio is there any good correspondence between the actual and the theoretical curves.

Graph IV illustrates the fact that the net driving ampere-turns is non-zero when the core is driven into saturation. For the MF-1131 (F262) core, an $(NI)_{net}$ of three ampere-turns suffices to drive the core from the remanent state at $-\phi_r$ to that of positive saturation at $+\phi_m$. The importance of this variable stems from the fact that, for the ferritic core, it determines the degree of switching.

Before interpreting the data for the three selected switch-core transformers, it is necessary that we derive a few more relations. Noting that both N_1 and N_2 are greater than four, one would expect that equation 3.7b would govern the relation between I_2 and I_1 so long as the core is not driven to saturation. In the saturated region, a different relation should be expected since in that region the two windings of the core are virtually decoupled. Referring to the usual definition of the coefficient of coupling, we see that

$$k = \frac{M}{\sqrt{L_1 \ L_2}} . \qquad (3.8)$$

In the unsaturated region, equation 3.7b states

$$\frac{I_2}{I_1} = \frac{M}{L_2}$$

$$= \frac{k \sqrt{L_1 \ L_2}}{L_2}$$

$$= k \frac{N_1}{N_2} = ka$$

or

$$k = \frac{N_2 \ I_2}{N_1 \ I_1} \qquad (3.9)$$

3.02 Interpretation of Data (Cont.)

A first-order approximation one might make is that the behavior of the core is governed by two linear relations between I_2 and I_1 -- one holding when the core is unsaturated; the second, when saturated. The transfer characteristic, i_2 (t): i_1 (t) of the core (with "many" turns) might then be represented by the polygonal line shown in Figure 8. For I_1 less than that required for saturation (with a given N_1), the characteristic is a straight line with slope $k_\alpha a$ where $k_\alpha \approx 0.95$; while for I_1 sufficient for saturation, one with slope $k_\beta a$ where $k_\beta \approx 0.05$.
At this point we may remark that the polygonal line of Figure 8 does resemble the curves of the average plate characteristics of a pentode. It was this resemblance that prompted D. A. Buck to suggest that one might utilize this characteristic in developing a magnetic-core constant-current generator.

Referring now to equation 3.1 we see that this may be written

$$(NI)_{net} = (1 - k_\beta)\ N_1\ I_1 \qquad (3.1a)$$

when the core material is saturated. Thus for a given value of N_1, there should be a linear relation between the net driving mmf and the primary current.

Applying the analytic relations to the experimental curves of Graphs V and VI, we note that these show plots of I_2 and of $(NI)_{net}$, respectively, as functions of I_1 for the selected combinations of N_1 and N_2. In the first graph, the actual and the ideal curves very nearly coincide over a limited range of I_1. In this region, the coefficient of coupling is approximately unity. For the turns used, k_α varies between 0.94 and 0.99. When the core is driven into saturation however, I_2 increases very slightly with increasing I_1. In this region, where the two windings are nearly independent of each other, the coefficient of coupling is nearly zero. The experimental data indicates that k_β is no greater than 0.075 for any of the turns used.

Graph VI also shows close agreement between theoretical and experimental results. Each of the three cores shows a linear relation between the net driving mmf and primary current when the core material is in a saturated state. If these lines are extrapolated linearly to the zero I_1 axis, they appear to intersect at a common point: --at $(NI)_{net} = - N_2 I_2 \approx - 15$ ampere-turns.

With this background of the behavior of saturable-core transformers with "many" turns, we can now examine the case with "few" turns. Since construction of a matrix switch is greatly simplified when the core elements have windings with relatively few turns, it is important to determine whether such a switch will work and, if so, what constraints are imposed on the vacuum tube drivers by going to "few" turns. The investigations in the second of our three sets of experiments were meant to provide some of the answers to these questions.

3.02 Interpretation of Data (Cont.)

Since it is neither desirable nor necessary to present all of the data collected, we include only that portion which will indicate trends. Thus, in Graphs VII and IX are shown plots of peak secondary current versus secondary turns and primary current respectively, when primary turns are held constant at $N_1 = 4$ turns; while in Graphs VIII and X are shown the same plots for $N_1 = 8$ turns.

From Graphs VII and VIII, we see that the forms of the curves are similar to those predictable from equations 3.7b and 3.7c. However, we note that rather heavy currents are required from the v.t. drivers preceding the cores if we are to have appreciable output current. Instead of the 400 milliamperes primary current which sufficed in the earlier experiments, we now require that the v.t. driver supply currents of the order of amperes.

In Graphs IX and X we observe that, although a linear relation still exists between I_2 and I_1, there are serious discrepancies between the actual and the ideal curves. These discrepancies decrease as either N_1 or N_2 are increased. It should be noted that by "ideal" we mean that equation 3.7b holds between I_2 and I_1. The actual data conforms more nearly to that of equation 3.7c.

The discrepancies noted thus far are brought home even more forcibly by Graphs XI and XII. There are depicted plots of I_2 versus I_1 with N_2 held constant and various values of turns ratios. In the first we see the case when $N_2 = 1$ turn; in the second, $N_2 = 4$ turns. From these it is apparent that going to few turns per winding results in a gain in simplicity of construction at the expense of a loss in effectiveness as a transformer.

The last set of experiments, involving static hysteresis loop measurements, derives its importance from the fact that this loop indicates the path of state of the material in the absence of eddy currents. To facilitate analysis, we might replace the actual "half-loop" (from the remanent flux density at $-B_r$ to positive saturation at $+B_m$) by a polygonal line of three segments. The first, at H = 0, has a slope

$$\mu_1 = \left.\frac{dB}{dH}\right|_{H = 0} ;$$

The second, at $H = H_c$ (coercive force), has a slope

$$\mu_2 = \left.\frac{dB}{dH}\right|_{H = H_c} ;$$

and the third, for saturation mmf, has the same slope as at H = 0. Below is shown a table of typical slopes for the saturation loops of the ferritic materials under discussion.

3.02 Interpretation of Data (Cont.)

Core Material	μ_1 (gauss/oersted)	μ_2 (gauss/oersted)
MF1131(F262)	60	3000
MF1118(F259)	40	2000

The self inductance of a toroidal core is, by equation 3.5,

$$L_a = \frac{2\mu_2 A}{r} \qquad N^2 = K_1 N^2$$

For an MF-1131 (F262) core operating in the vicinity of $H = H_c$,

$$\mu_2 = 3000 \text{ gauss/oersted}$$
$$r = 0.333 \text{ cm}$$
$$A = 0.14 \text{ cm}^2 \quad ;$$

so that

$$L_a = 2.52 N^2 \text{ microhenries.}$$

For an MF-1118 (F259) core operating in the vicinity of H = 0,

$$\mu_1 = 40 \text{ gauss/oersted}$$
$$r = 0.214 \text{ cm}$$
$$A = 0.0154 \text{ cm}^2 \quad ;$$

so that

$$L_b = 0.00575 N^2 \text{ microhenries/core}$$

When operated in the memory array (in the mode used throughout our experiments), these memory cores are connected, all 256 in series, by a single wire. Hence the equivalent inductance of the array due to the cores alone is

$$L_{eq} = 256 \ (0.00575 \ \mu h/\text{core})$$
$$= 1.47 \ \mu h$$

When one adds to this the leakage inductance of the wire between cores (which is probably of the order of one microhenry), one sees that this result is in good agreement with that empirically derived by W. Ogden and E. Guditz. Using inductors with nominal ratings, they matched the response of a dummy load with that of the Z-plane of the array and found that a one ohm resistor in series with a two microhenry inductor gave a good match.

4.0 Conclusions

From the results presented above, some rather important conclusions may be drawn:

(a) If ferritic core material is used for switching applications and if the core is not driven far into saturation, then the

4.0 Conclusions (Cont.)

behavior of the switch elements may be described in terms of linear coupled-circuit theory. Although a more adequate model (at pulse frequencies) should include capacitive effects, it is encouraging to observe that a rather simple model may be used to interpret experimental results.

(b) Simplicity of construction of a matrix switch can be obtained only at a loss in effectiveness of transformer action. The overriding importance of simplicity of construction may constrain the design to relatively few turns per winding (at least on the primary windings). Since the trend in memory cores is toward a smaller core body (e.g., die size F-291) with the attendant smaller current requirements, this loss in effectiveness may be one which we are willing to accept.

(c) The near absence of eddy currents suggests that the static hysteresis loop may be used to describe the path of magnetic state of the material even at pulse frequencies, and hence to facilitate the analytical work involved in a matrix switch design.

Signed: A. Katz
A. Katz

Signed: Elis A. Guditz
E. A. Guditz

Approved: WNP
W. N. Papian

AK:EAG/aik

Please attach these drawings to your copy of E-500.

"Switch-Core Analysis I" by A. Katz and A. Guditz.

Thank You.

Print Room - Whittemore

B-50910
F-1470
SN-372

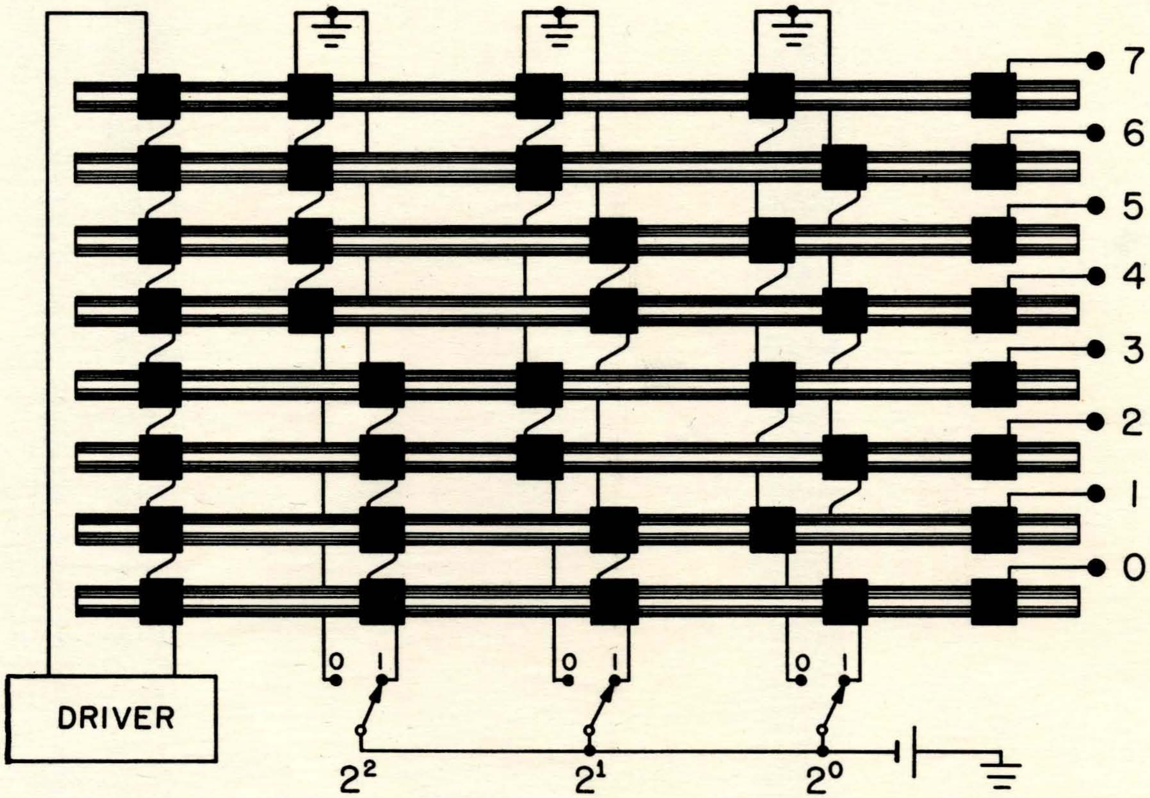

8-POSITION MAGNETIC-MATRIX SWITCH

FIG. 1

A-52936

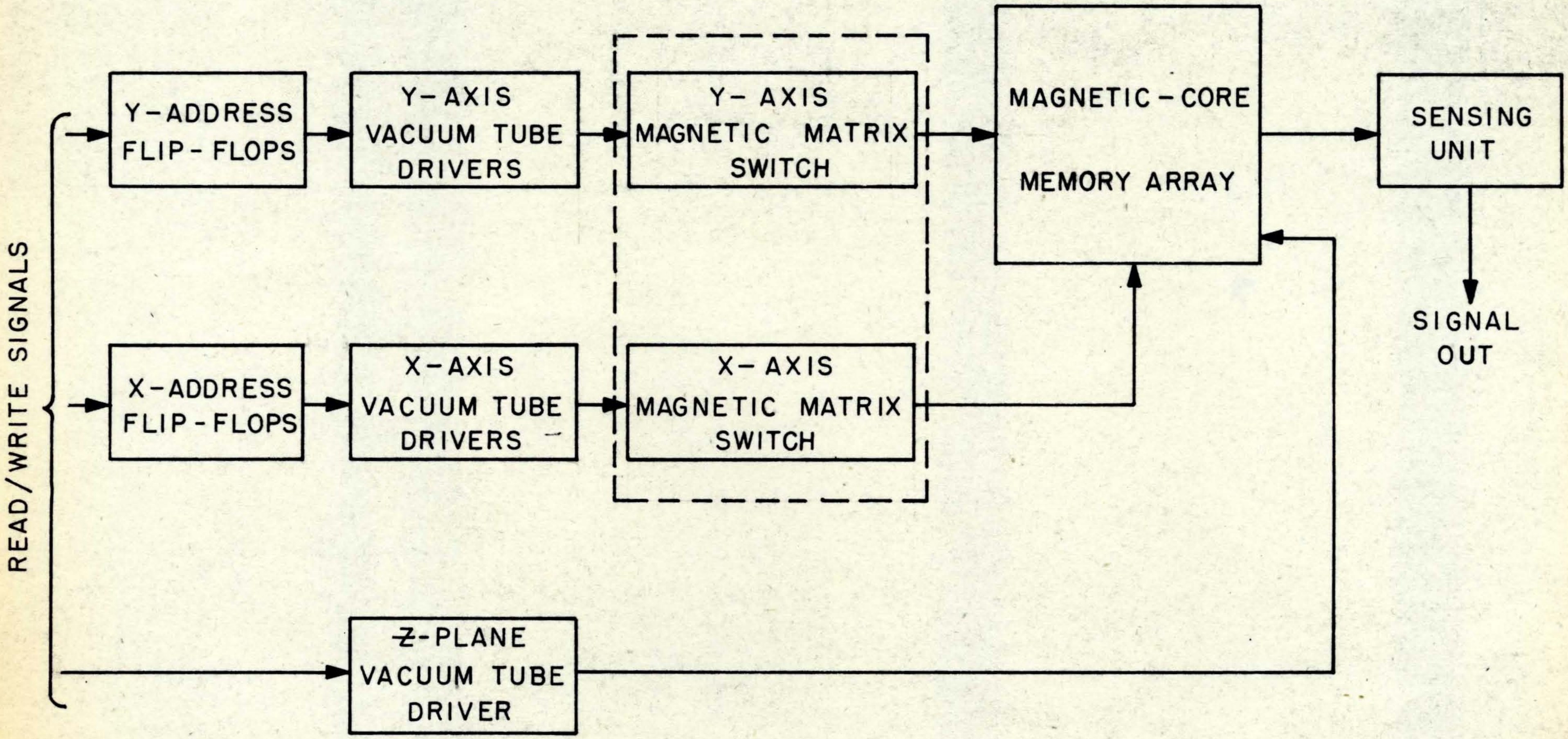

FIG. 2

A SELECTION SYSTEM FOR A MAGNETIC-CORE MEMORY ARRAY

A-52934

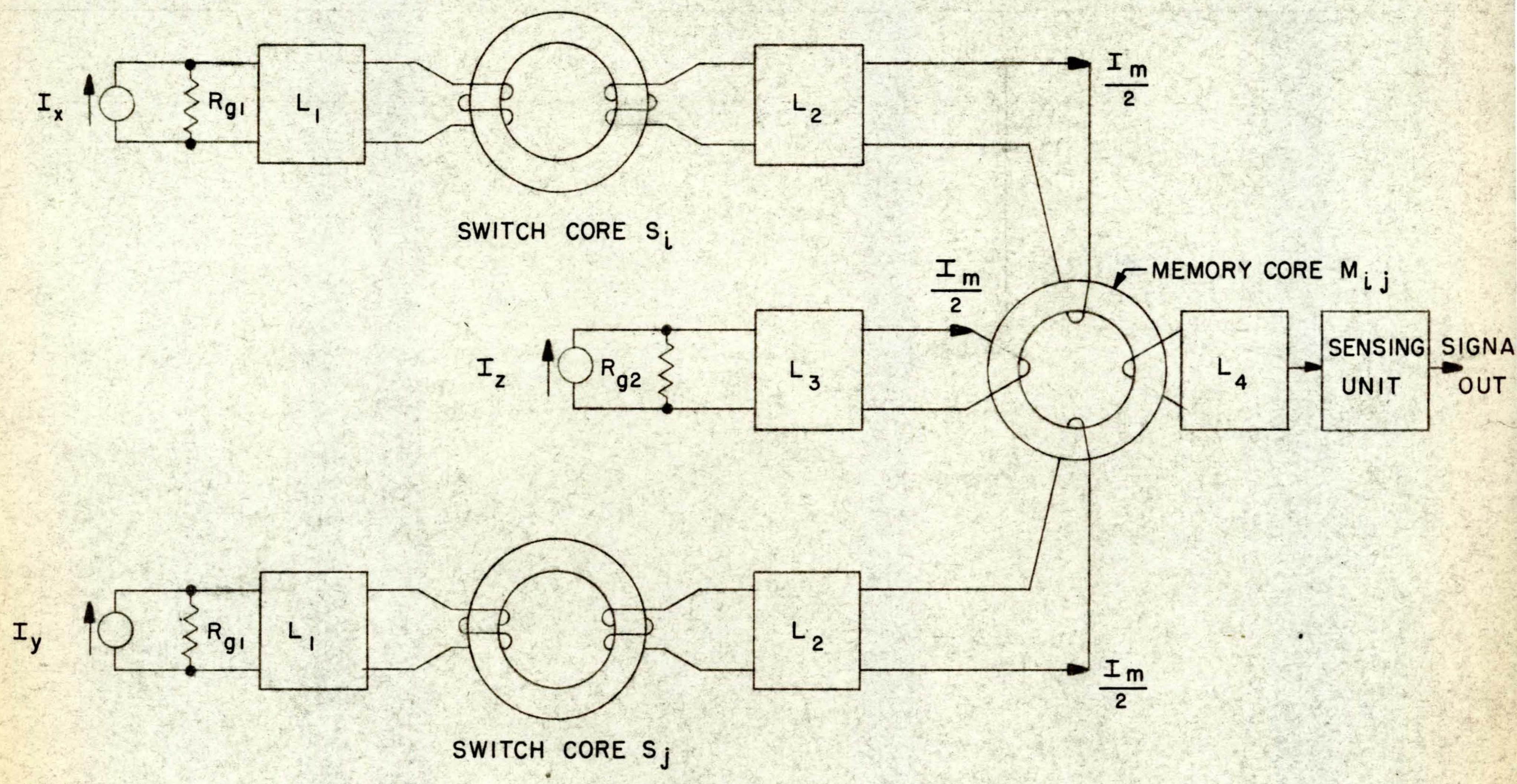

FIG. 3

ESSENTIAL ELEMENTS OF A SWITCH-CORE DRIVEN MAGNETIC MEMORY ARRAY

A-52940

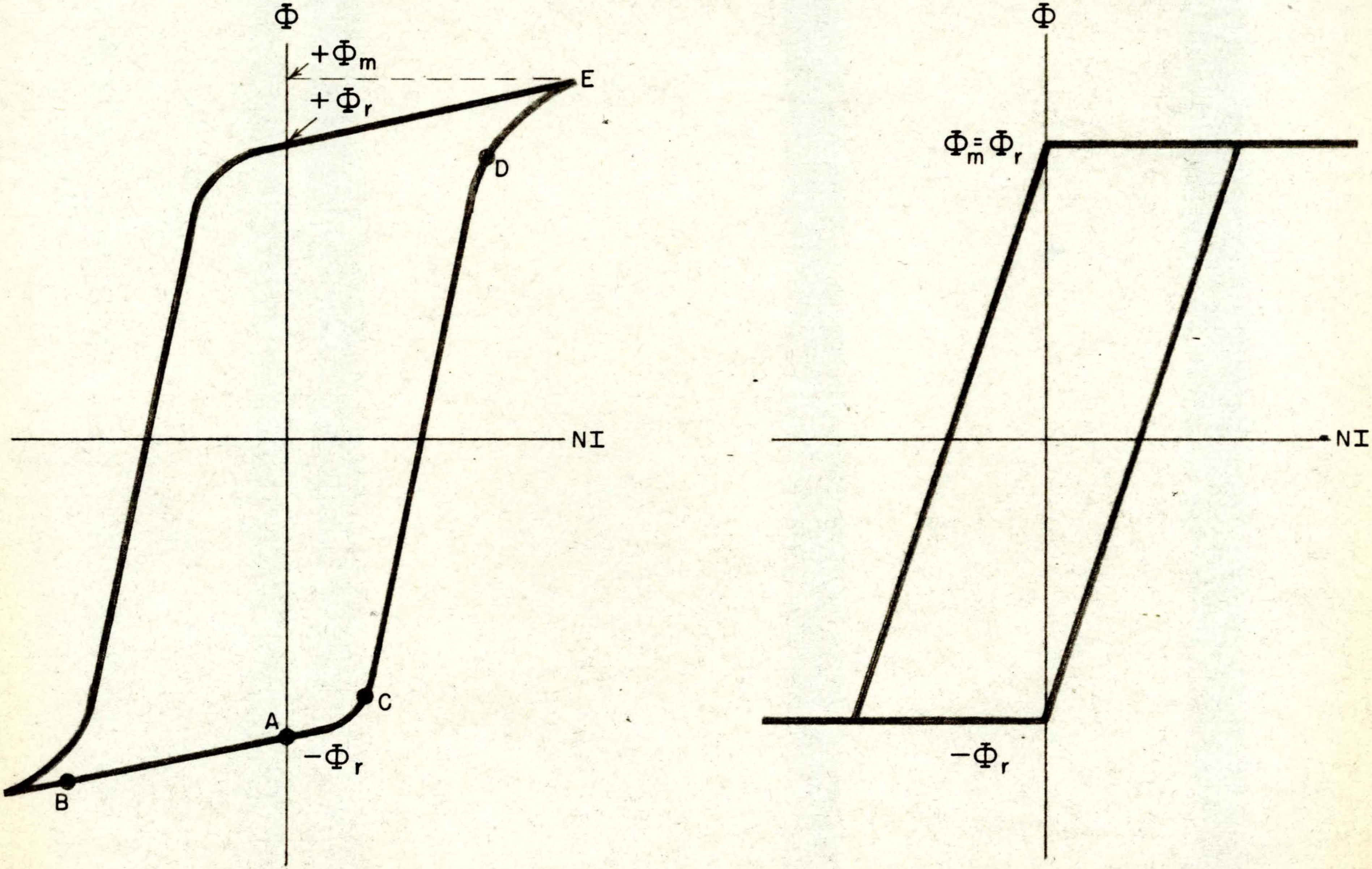

a) ACTUAL SWITCH CORE

b) IDEAL SWITCH CORE

FIG. 4

STATIC HYSTERESIS CURVES FOR RECTANGULAR-LOOP CORE MATERIALS

A-52932

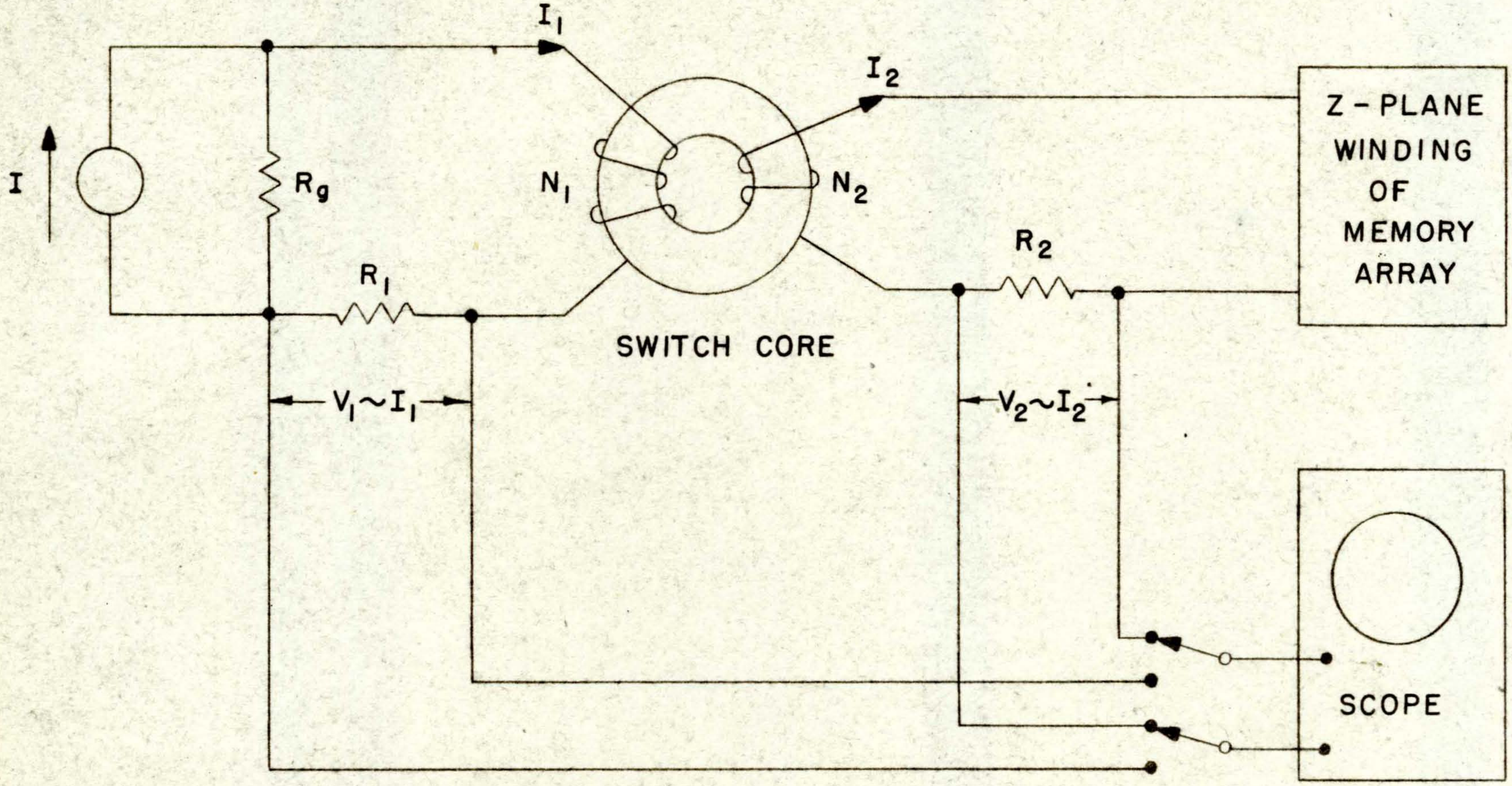

FIG. 5

TEST SET-UP FOR STUDY OF SWITCH CORES

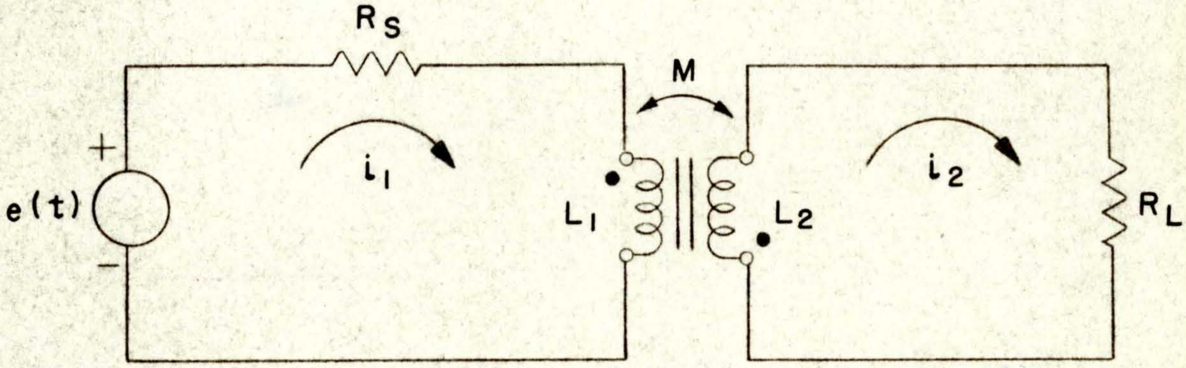

L_1 = PRIMARY SELF-INDUCTANCE
L_2 = SECONDARY SELF-INDUCTANCE
M = MUTUAL INDUCTANCE
R_S = SOURCE RESISTANCE
R_L = LOAD RESISTANCE

FIG. 6

IRON-CORE COUPLED CIRCUIT

A-52933

A-52950

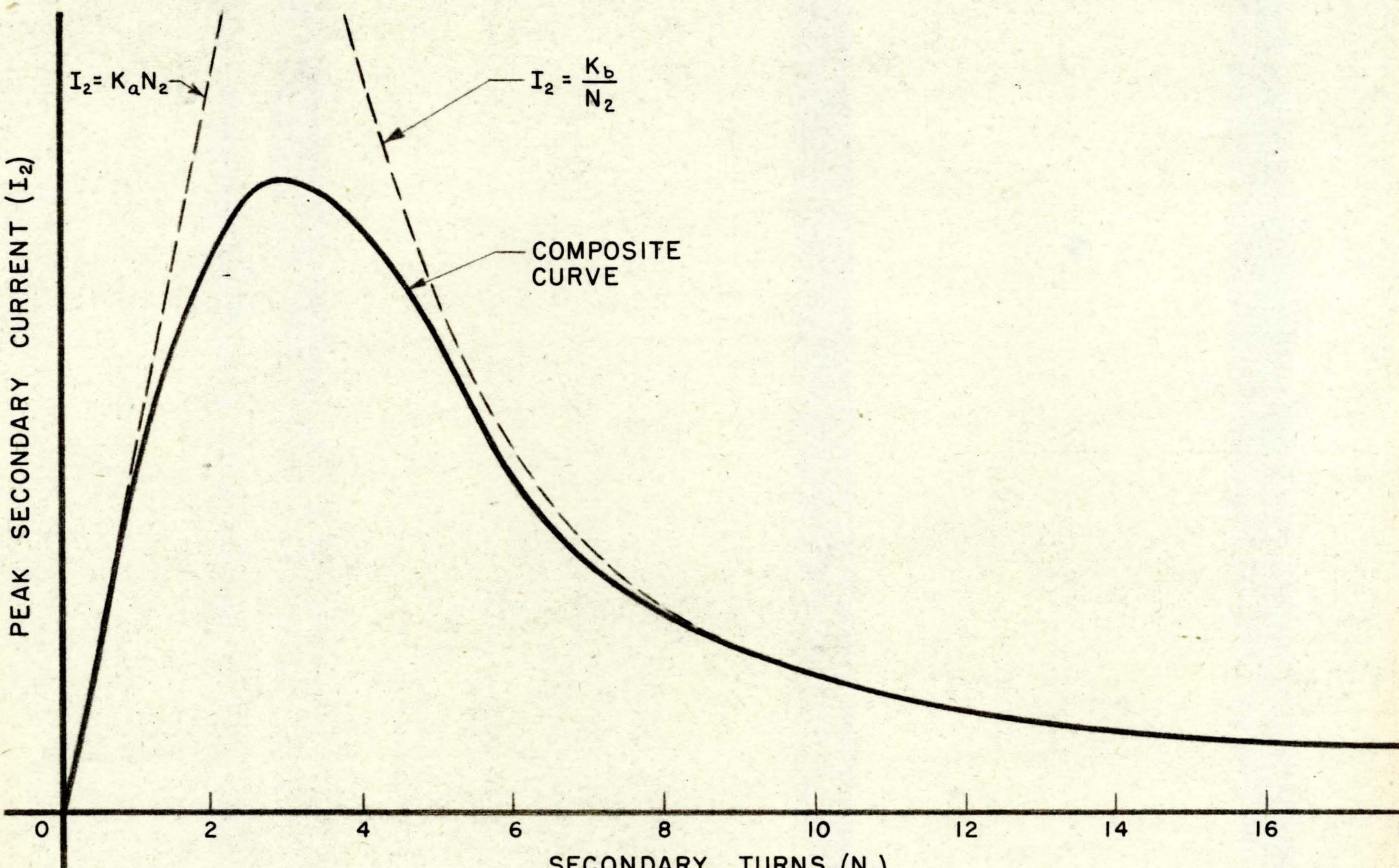

FIG. 7

PREDICTED CURVE OF PEAK SECONDARY CURRENT VERSUS SECONDARY TURNS FOR CONSTANT PRIMARY AMPERE-TURNS

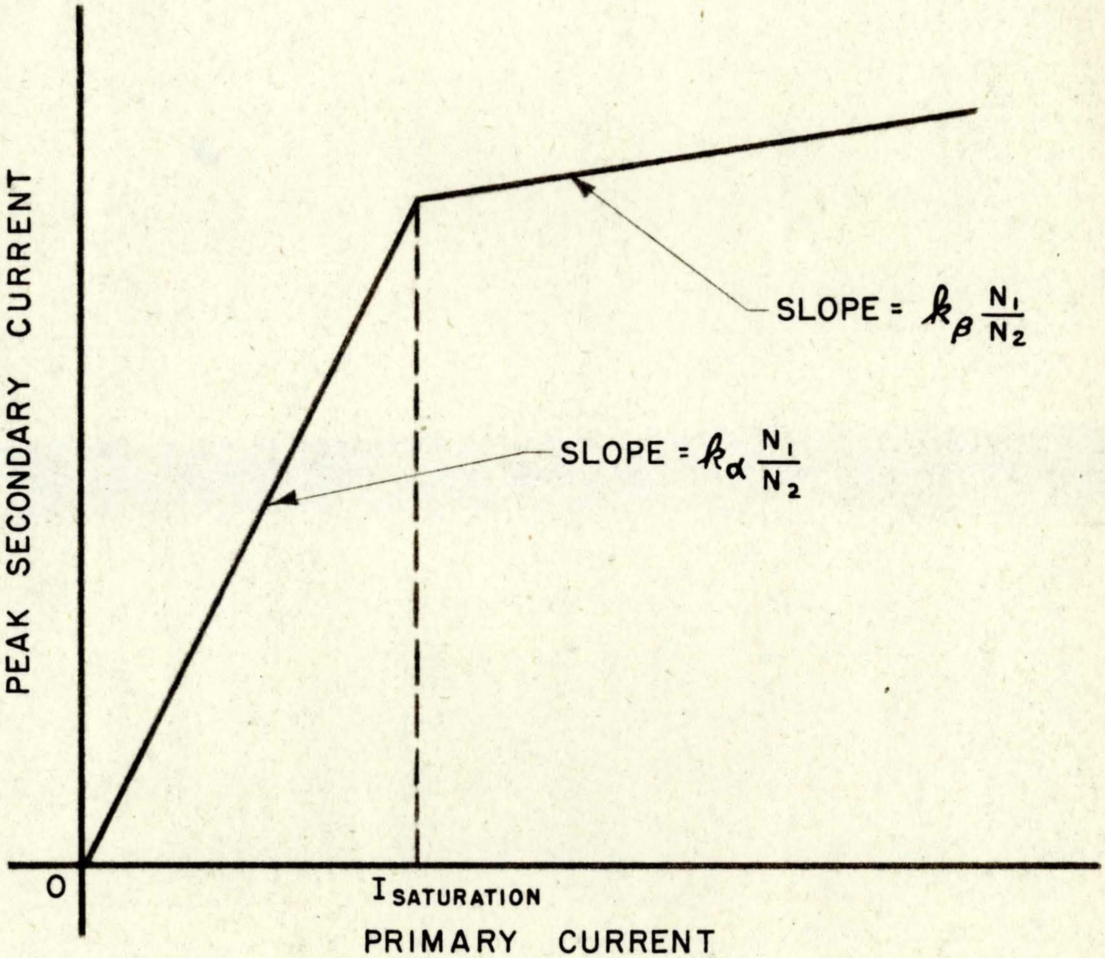

FIG. 8

APPROXIMATE TRANSFER CHARACTERISTIC
FOR SWITCH-CORE WITH "MANY" TURNS

A-52951

SA-48378-G

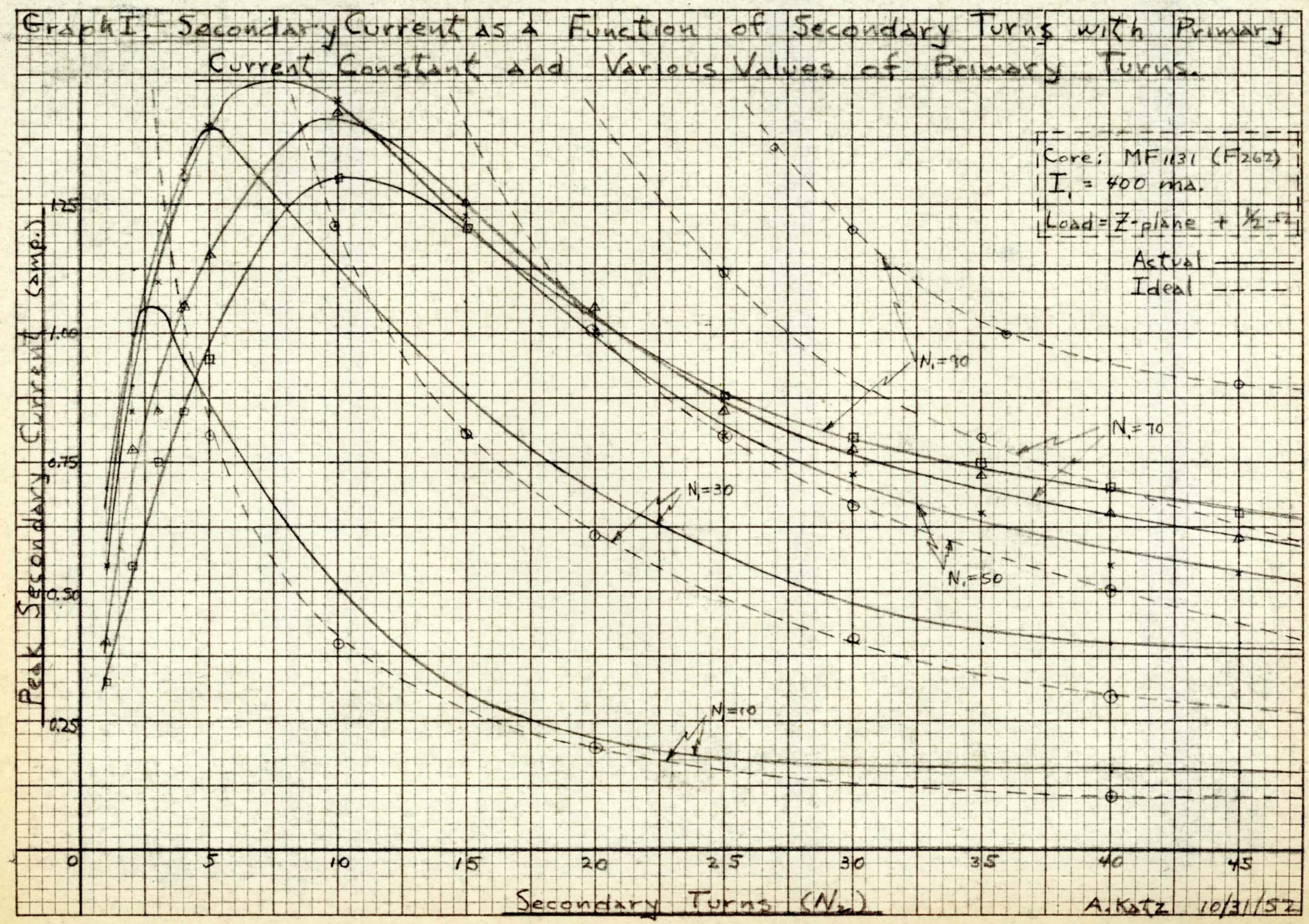
Graph I – Secondary Current as a Function of Secondary Turns with Primary Current Constant and Various Values of Primary Turns.
Core: MF 1131 (F262)
I_1 = 400 ma.
Load = Z-plane + ½ Ω
Actual
Ideal
N_1=90
N_1=70
N_1=50
N_1=30
N_1=10
Peak Secondary Current (amp.)
1.25
1.00
0.75
0.50
0.25
0
5
10
15
20
25
30
35
40
45
Secondary Turns (N_2)
A. Katz 10/31/52

SA-48379-G

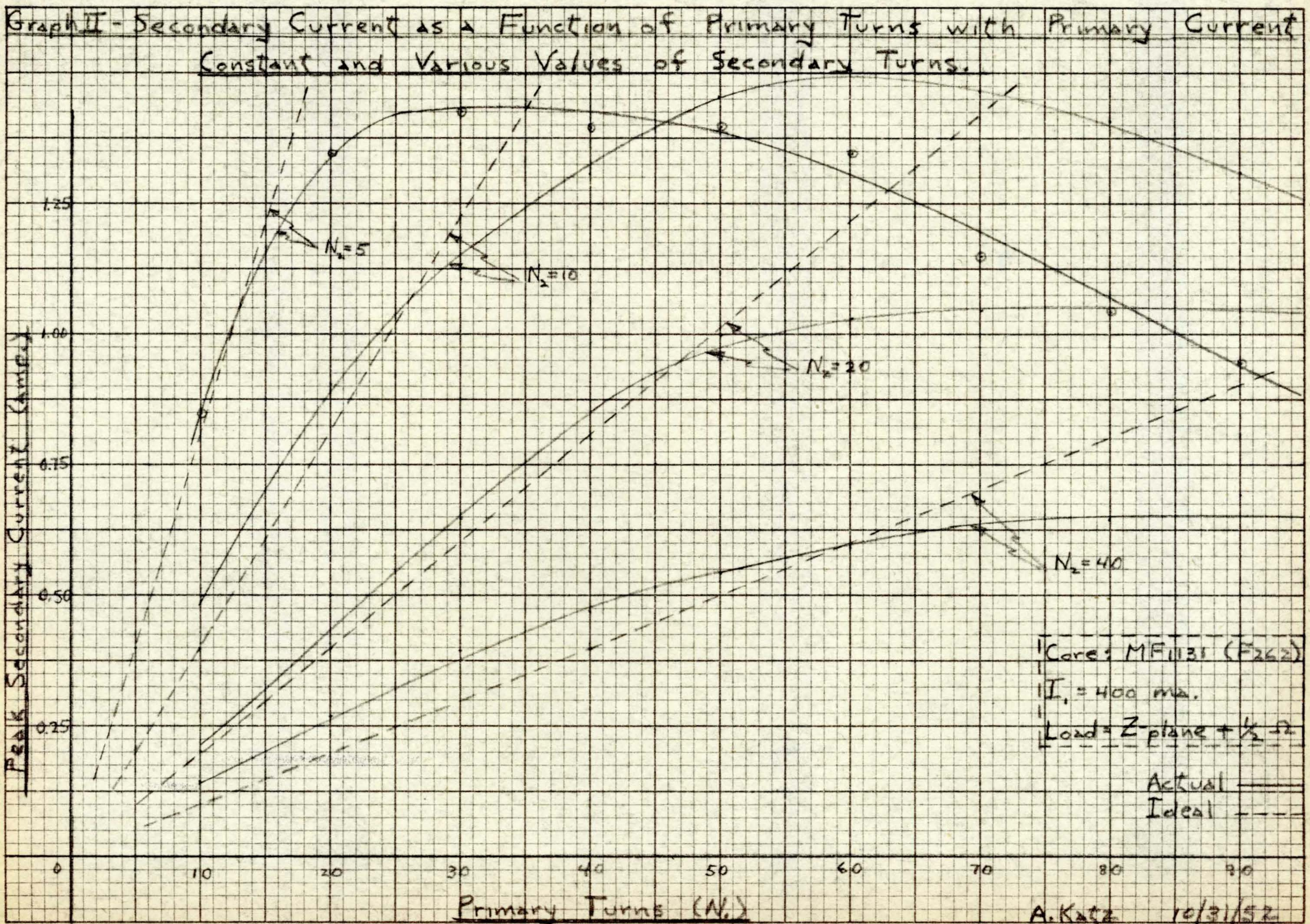
Graph II - Secondary Current as a Function of Primary Turns with Primary Current Constant and Various Values of Secondary Turns.
Peak Secondary Current (Amps.)
1.25
1.00
0.75
0.50
0.25
0
10
20
30
40
50
60
70
80
90
Primary Turns (N₁)
$N_2 = 5$
$N_2 = 10$
$N_2 = 20$
$N_2 = 40$
Core: MF1131 (F262)
I_1 = 400 ma.
Load = Z-plane + ½ Ω
Actual
Ideal
A. Katz 10/31/52

SA-48380-G

Graph III - Secondary Current as a Function of Secondary Turns with Primary Current Constant and Various Values of Turns Ratios.

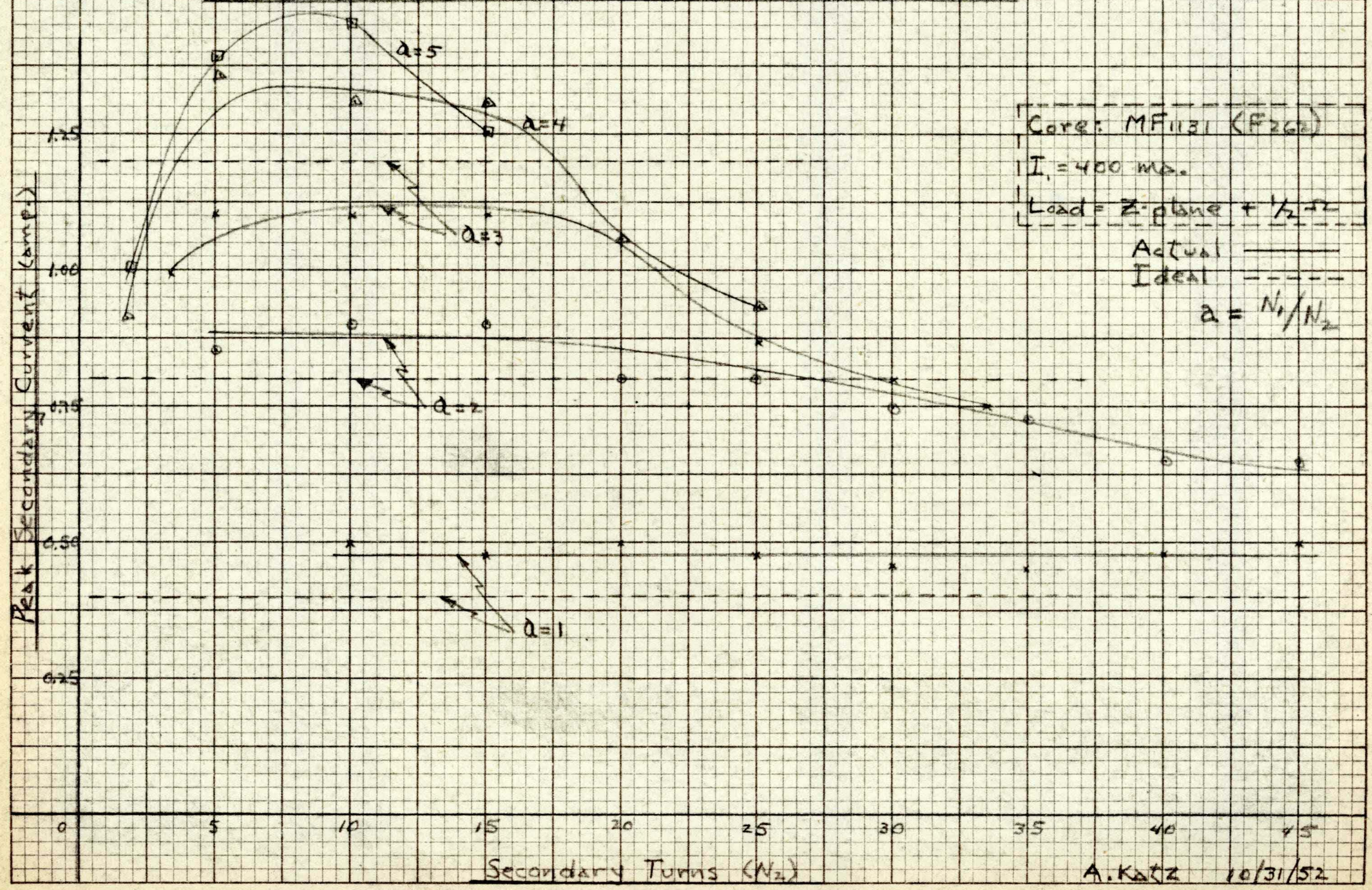

A. Katz 10/31/52

SA-48381-G

359T-6G KEUFFEL & ESSER CO.
5 × 5 to the ½ inch.
MADE IN U. S. A.

Graph IV. - Net Ampere-Turns as a Function of Secondary Turns with Primary Current Constant and Various Values of Primary Turns.

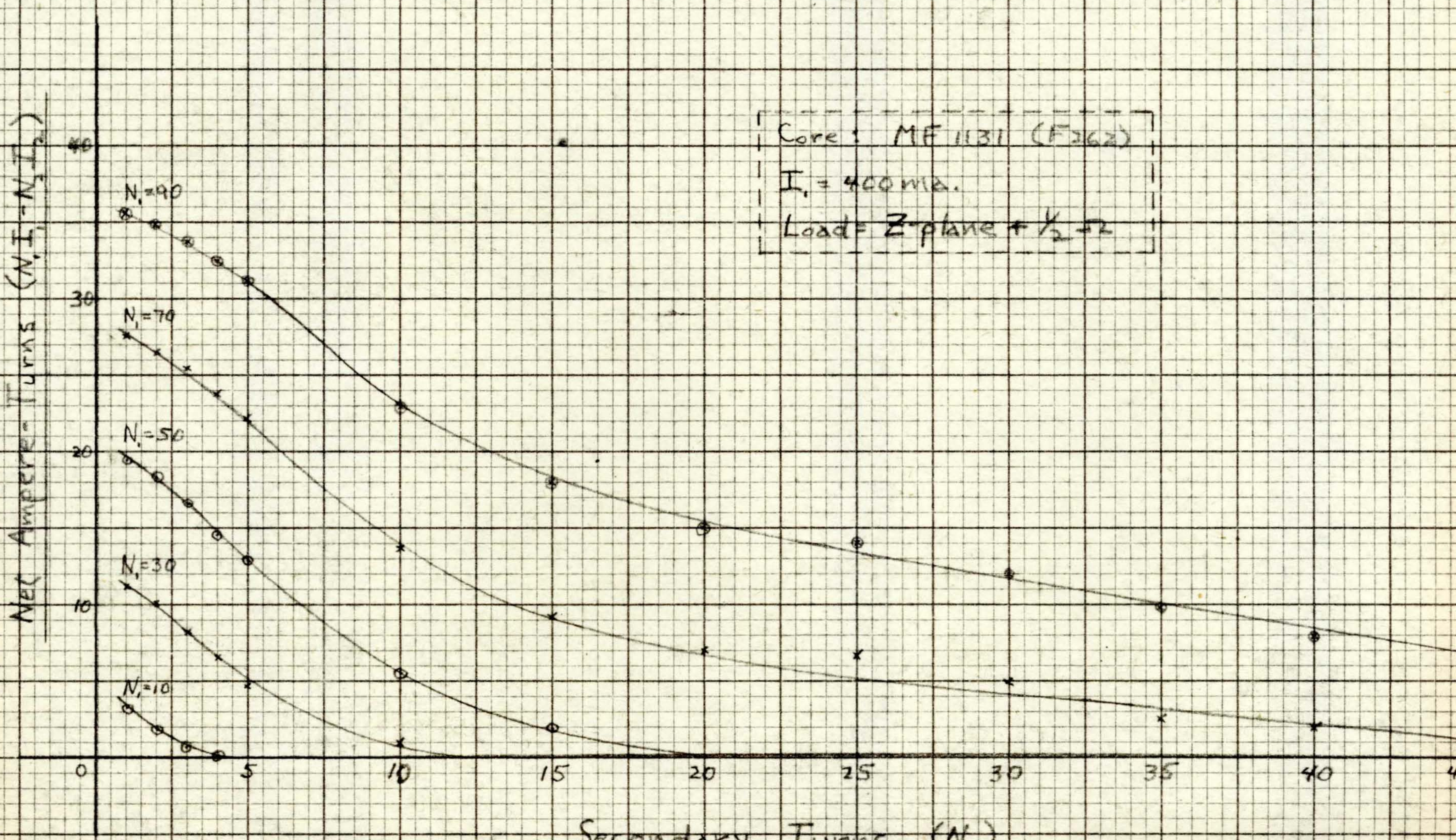

Secondary Turns (N_2)

A. Katz 10/31/52

Graph V - Secondary Current as a Function of Primary Current for Various Turns Ratios.

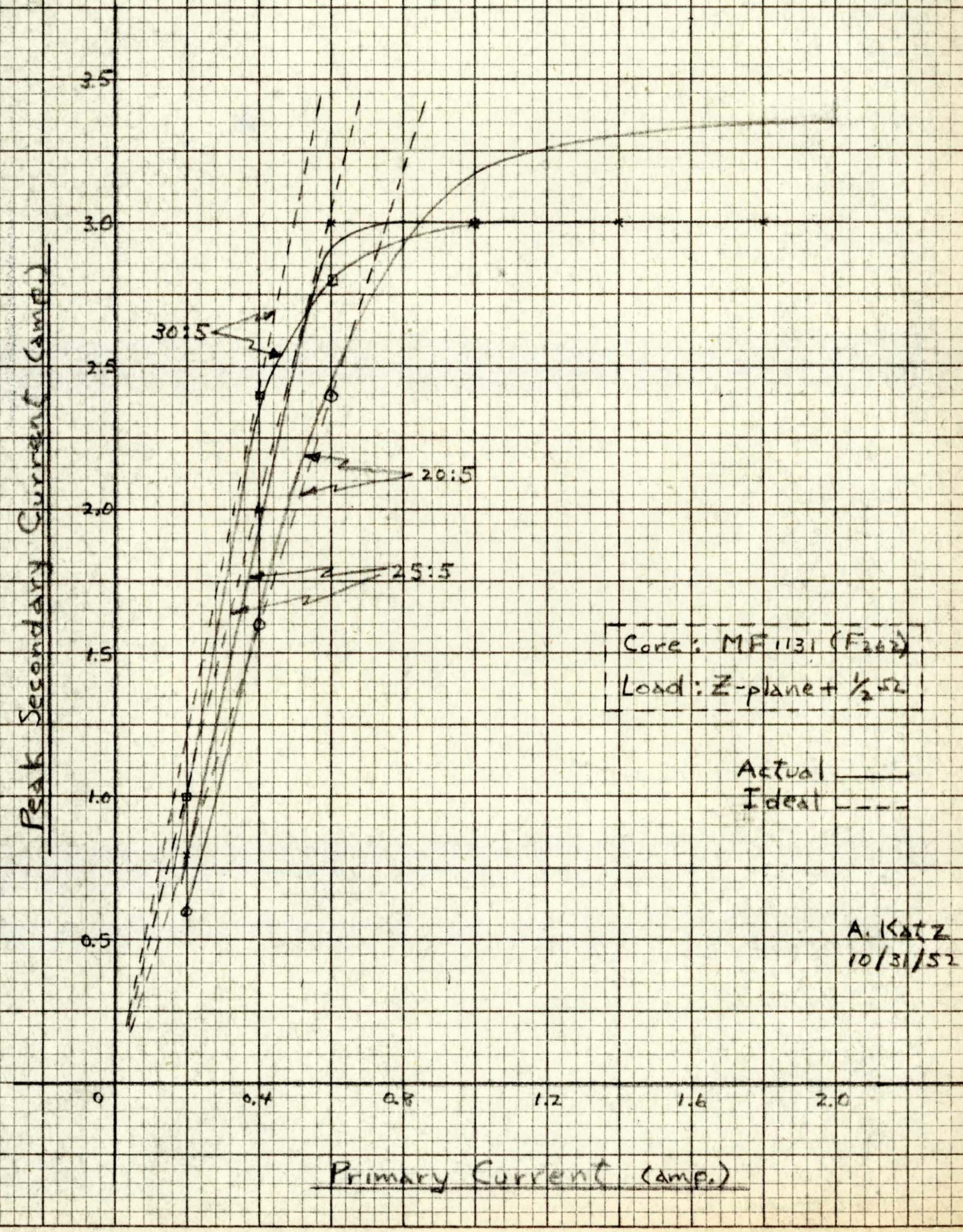

SA-48382-G

359T-6G KEUFFEL & ESSER CO. 5 × 5 to the 1/2 inch. MADE IN U.S.A.

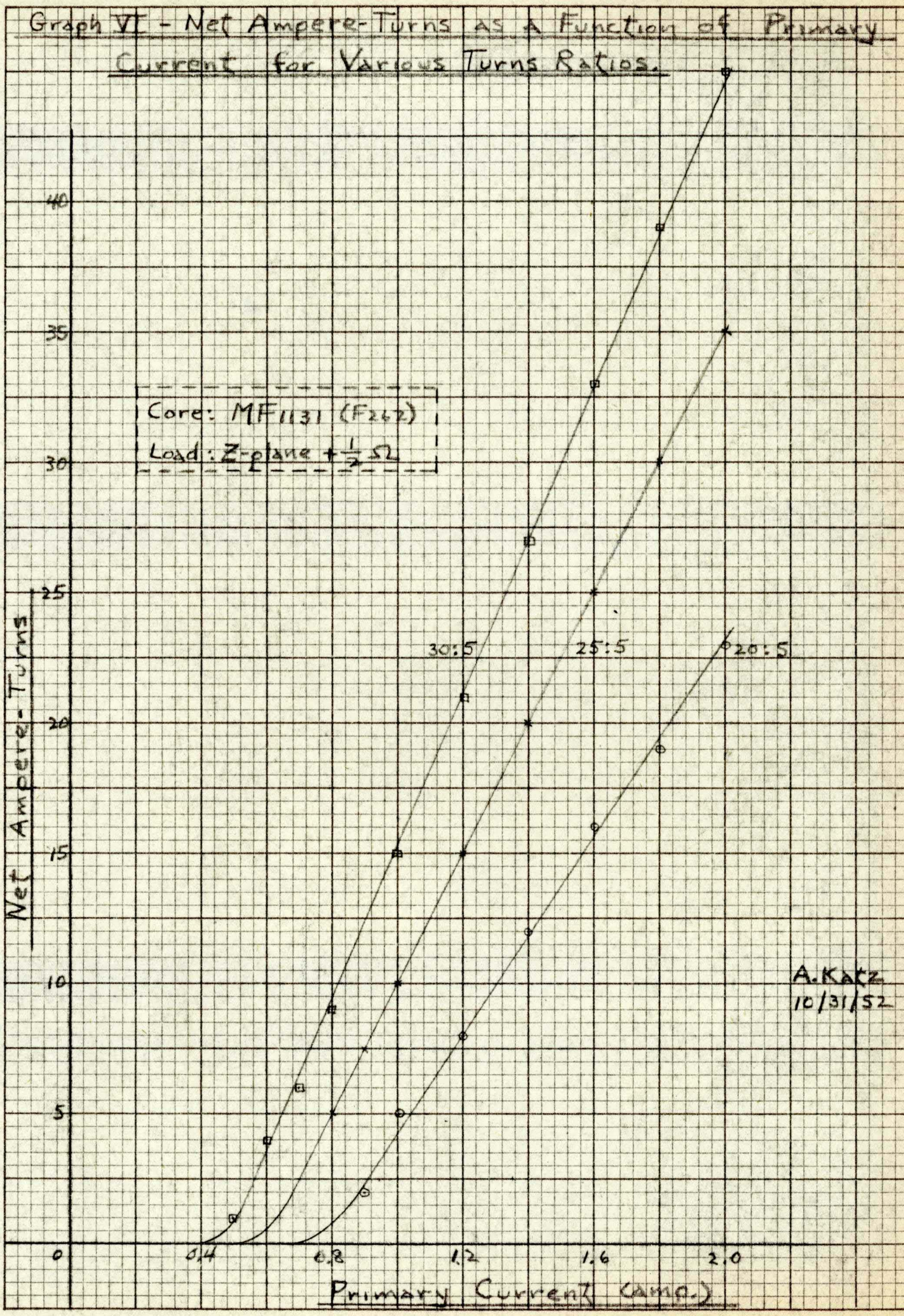

Graph VI - Net Ampere-Turns as a Function of Primary Current for Various Turns Ratios.
Core: MF1131 (F262)
Load: Z-plane + 1/2 Ω
Net Ampere-Turns
Primary Current (amp.)
30:5
25:5
20:5
0
5
10
15
20
25
30
35
40
0.4
0.8
1.2
1.6
2.0
A. Katz
10/31/52

SA-48383-G

SA-48384-G

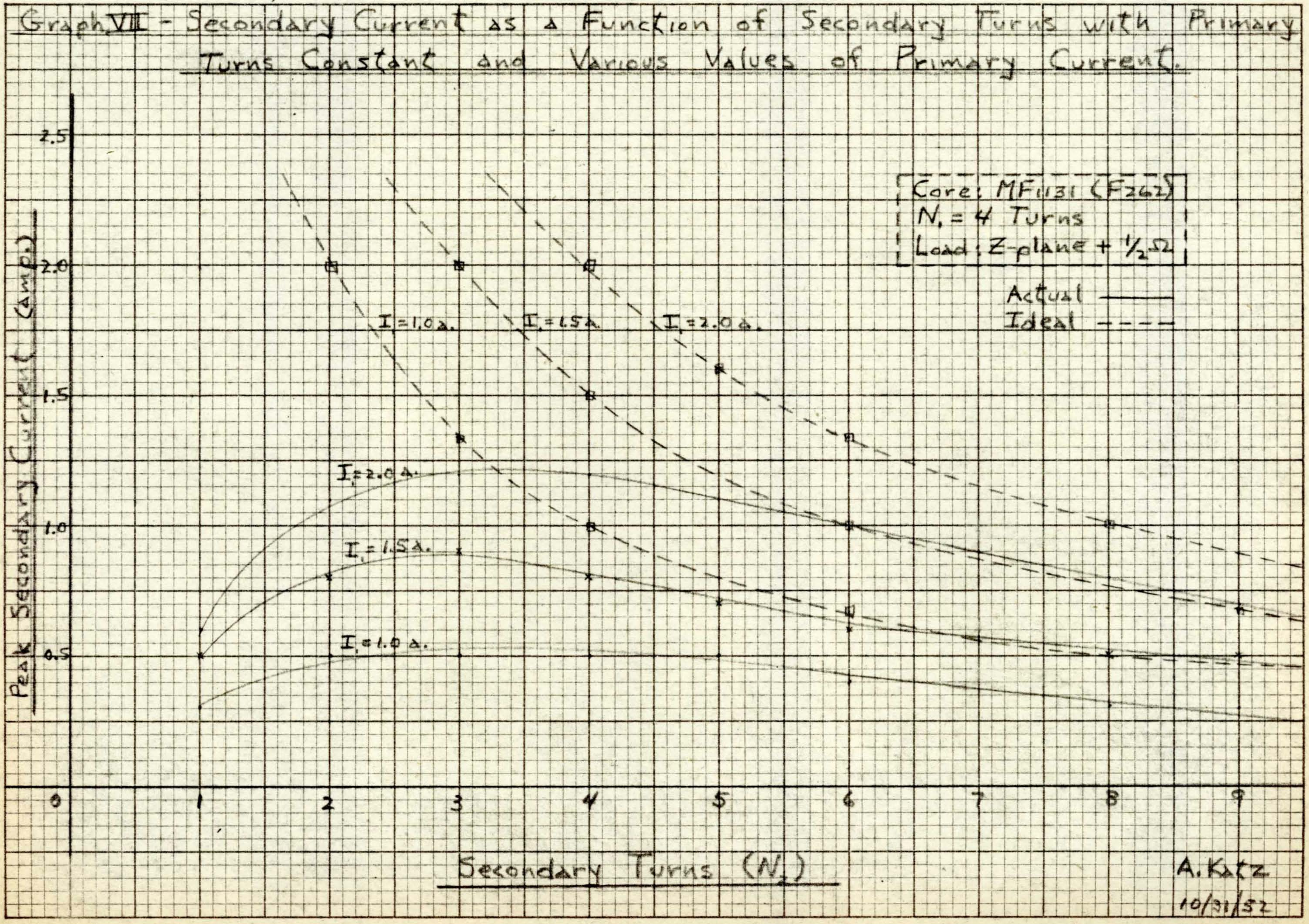
Graph VII - Secondary Current as a Function of Secondary Turns with Primary Turns Constant and Various Values of Primary Current.
Core: MF1131 (F262)
N1 = 4 Turns
Load: Z-plane + 1/2 Ω
Actual
Ideal
I1 = 1.0 a.
I1 = 1.5 a.
I1 = 2.0 a.
I1 = 2.0 a.
I1 = 1.5 a.
I1 = 1.0 a.
Peak Secondary Current (amp.)
2.5
2.0
1.5
1.0
0.5
0
1
2
3
4
5
6
7
8
9
Secondary Turns (N2)
A. Katz
10/31/52

SA-48385-G

Graph VIII. - Secondary Current as a Function of Secondary Turns with Primary Turns Constant ($N_1 = 8$), and Various Values of Primary Current.

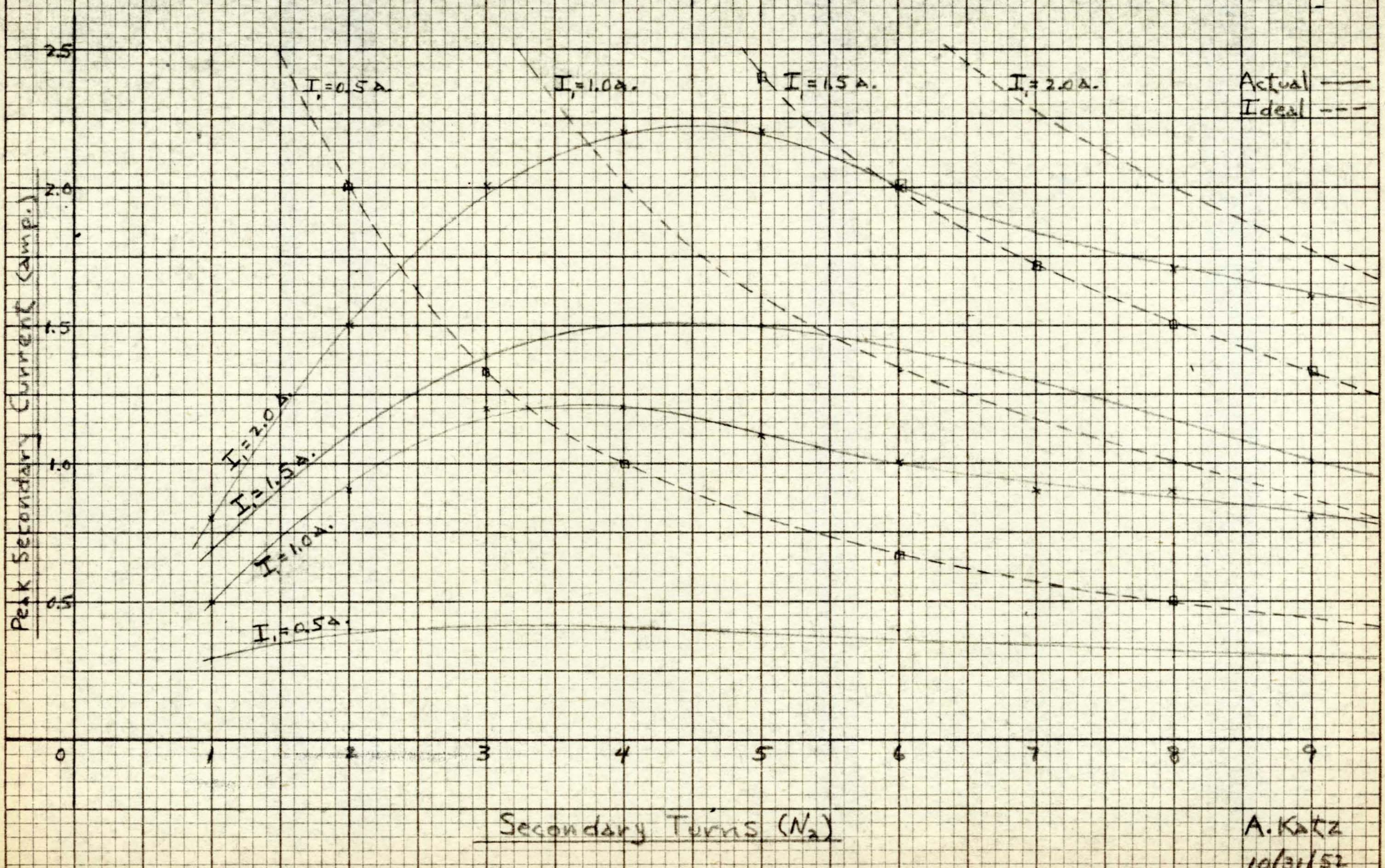

A. Katz
10/31/52

SA-48386-G

Graph IX. - Secondary Current as a Function of Primary Current with Primary Turns Constant and Various Values of Turns Ratios.

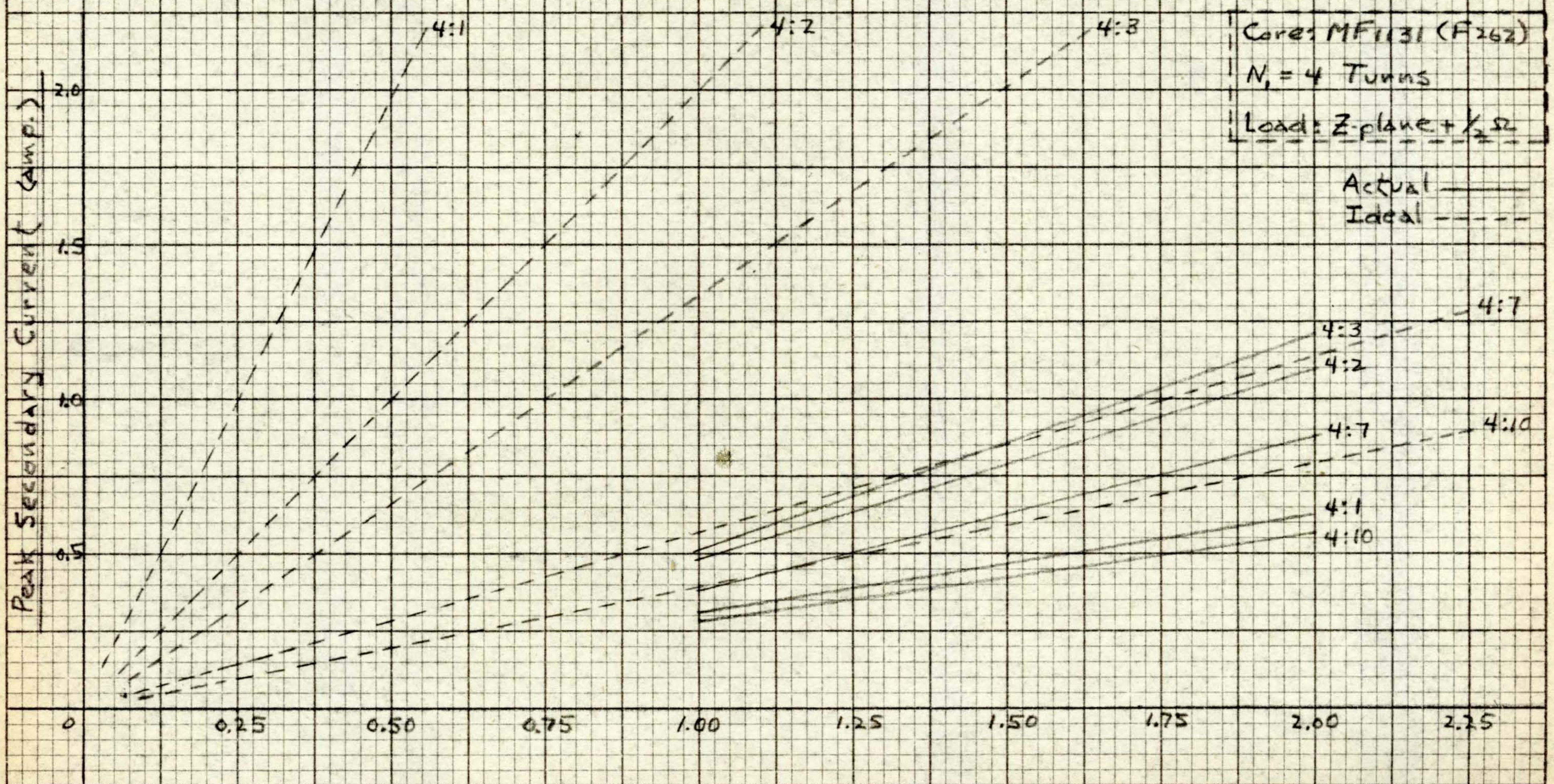

A. Katz
10/31/52

SA-48387-G

Graph X - Secondary Current as a Function of Primary Current with Primary Turns Constant ($N_1 = 8$) and Various Values of Turns Ratios.

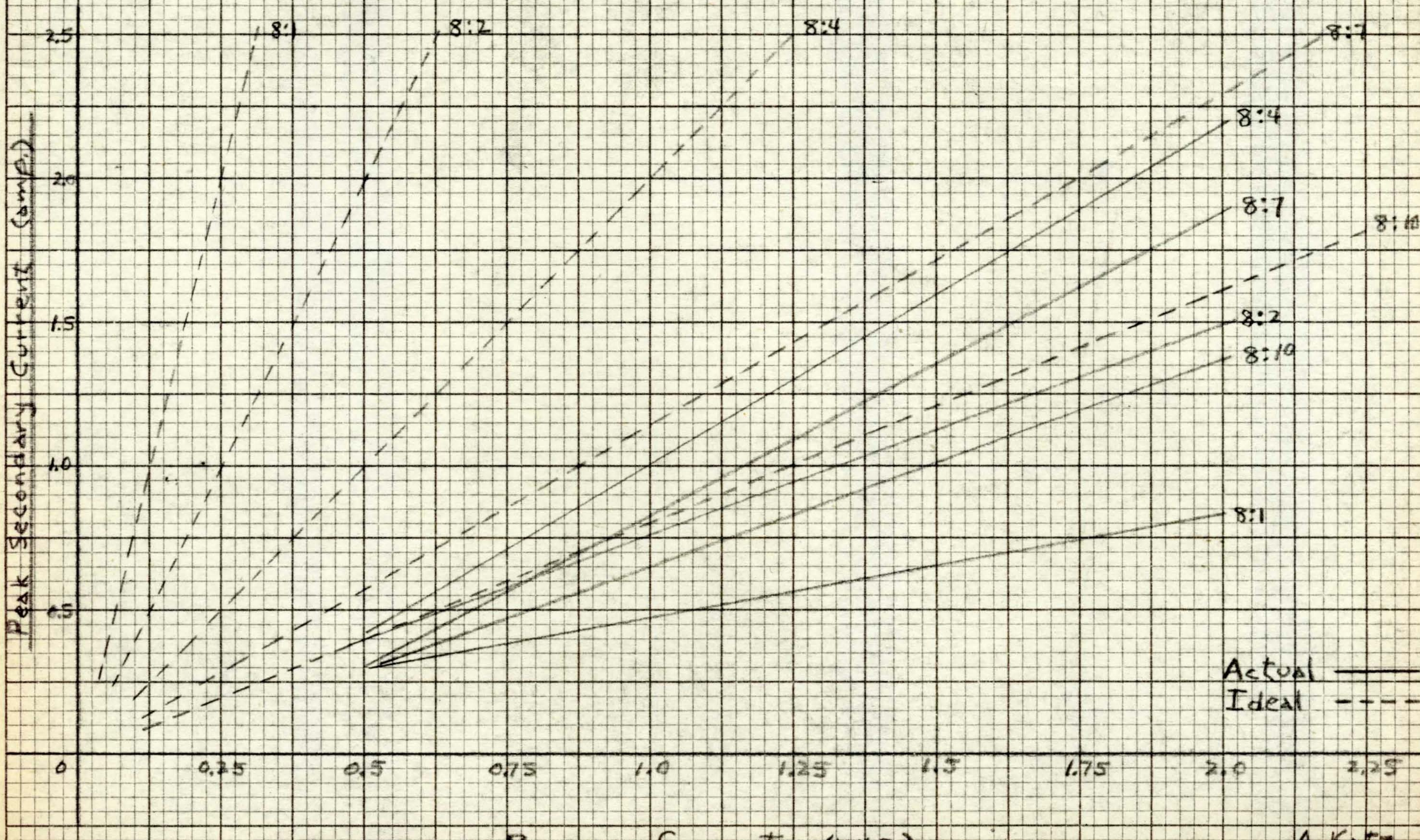

A. Katz
10/31/52

SA-48388-G

Graph XII - Secondary Current as a Function of Primary Current with Secondary Turns Constant ($N_2 = 1$) and Various Values of Turns Ratios.

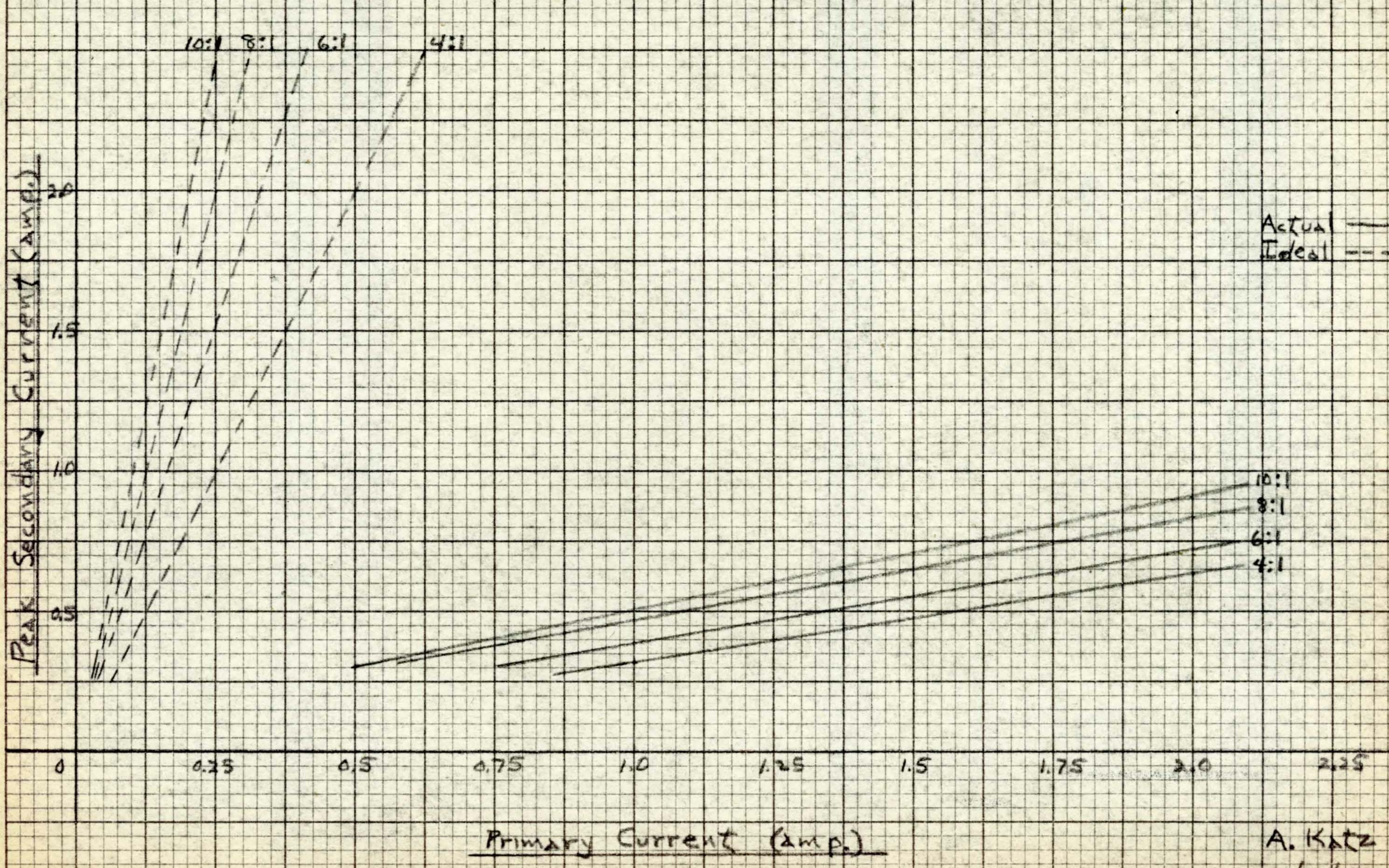

A. Katz
10/31/52

SA-48389-G

Graph XIII - Secondary Current as a Function of Primary Current with Secondary Turns Constant ($N_2 = 4$) and Various Values of Turns Ratios.

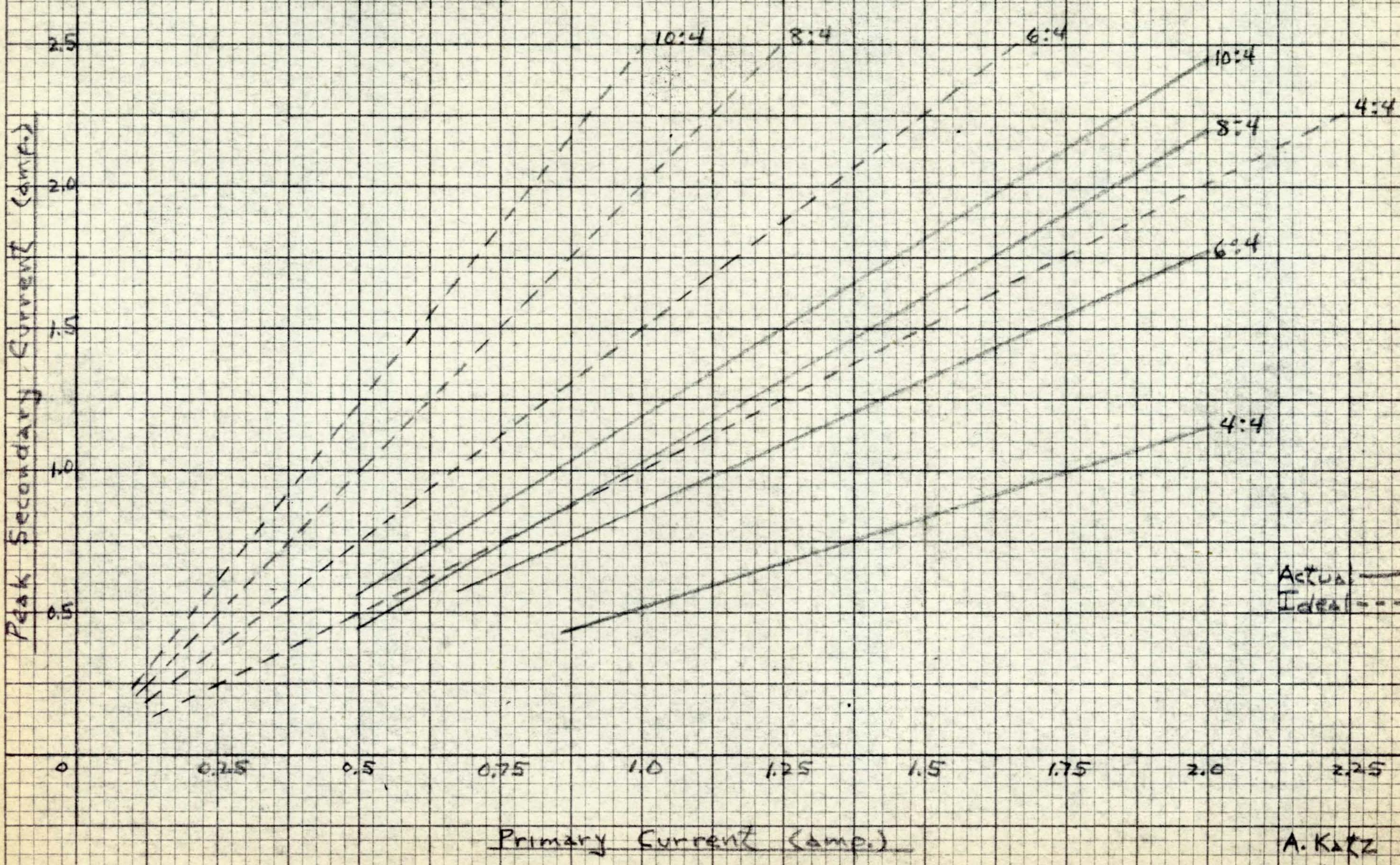

A. Katz
10/31/52